

## CHAPTER 3

---

# Corneal Topography Basics

One of the newest advanced-technology instruments that optometrists and ophthalmologists use to evaluate cornea and contact lens patients, is the computerized videokeratoscope. These devices are primarily being used to examine the cornea for subtle shape anomalies, such as keratoconus. Corneal surgeons are particularly concerned with keratoconus since its presence would contraindicate refractive surgery. The videokeratoscope also helps doctors manage corneal distortion in contact lens patients, and by using these instruments, it is possible to design contact lenses to precisely match each eye's corneal contour. This technology is relatively new, and I found that even among doctors who use corneal topography maps, there is considerable confusion about how to interpret the corneal maps actually show. To improve my understanding of this subject, I studied the underlying principles of corneal topography, and using theoretical cornea data, created examples of the various corneal maps that may be produced by modern videokeratoscopes. This exercise provided valuable insight into what these maps really show about the cornea and was organized into an article that was published in *Optometry and Vision Science* (Salmon & Horner, 1995). It was expanded and subsequently published as a chapter (Horner, Salmon, & Soni, 1998) in the 1998 edition of *Borish's Clinical Refraction*, a standard optometry textbook. Much of the information from these two publications is summarized in the following pages of this chapter and this provides background information for the research described in Chapters 4 and 5.

### 3.1

#### IMPORTANCE OF CORNEAL OPTICS

We should be able to learn much about the eye's aberrations from corneal topography since the anterior corneal surface is the primary refractive element in the eye. Fortunately, this very important optical surface is also easily accessible to noninvasive measurement. The corneal surface alone accounts for

about 70% of the eye's refractive power, and some reduced eye models, which use only a single refracting surface (a modified cornea), are able to simulate optical performance for the whole eye quite well (Thibos, 1987; Thibos, 1992; Thibos, Ye, Zhang, & Bradley, 1997). Scientists studying optical aberrations of the eye have long recognized that the asphericity of the cornea is a major factor that determines the amount of spherical aberration in the eye (Westheimer, 1963; Millodot & Sivak, 1979; Atchison, 1984).

Since the optical properties of a transparent surface are primarily determined by its shape, a detailed knowledge of corneal optics requires high quality surface topography data. For over 100 years keratometry has given clinicians a rough estimate of corneal shape based on data from four paracentral points. Thanks to recent advances in computer technology, we can now sample and process data for 5-10,000 points, and map the topography of the cornea to micrometer accuracy (Horner & Salmon, 1998). From the topographic data, it is possible to calculate sophisticated measures of optical performance (Camp, Maguire, Cameron, & Robb, 1990; Maguire, Zabel, Parker, & L, 1991), including the corneal wavefront aberration function (Hemenger, Tomlinson, & Oliver, 1994; Oliver, Hemenger, Corbett, & al., 1997; Oshika, Klyce, Applegate, Howland, & El Danasoury, 1999). This advanced application of corneal topography may one day be included in the routine clinical evaluation of the eye's optical quality, but today corneal topography maps are mainly being used to detect anomalies of surface shape.

The measurement of corneal optics has clinical application to areas such as refractive surgery and high resolution retinal photography. In laser refractive surgery, the excimer laser vaporizes corneal tissue to reshape it into a new lens, thereby correcting the patient's refractive error. This is usually performed with no regard for induced optical aberrations (Camp, *et al.*, 1990; Stein, Cheskes, & Stein, 1995; Schwiegerling & Snyder, 1998), and often complicated aberrations result (Oliver, *et al.*, 1997; Oshika, *et al.*, 1999). Patients may experience reduced vision, especially with low contrast targets or in low illumination (Maguire, 1994; Verdon, Bullimore, & Maloney, 1996; Gauthier, *et al.*, 1998; Bullimore, Olson, & Maloney, 1999). By studying corneal topography, we can understand exactly how changes in surface shape affect optical quality.

The correct management of many retinal diseases depends on high quality fundus images of microscopic features (Kinyoun, *et al.*, 1989; Aiello, 1994), but these are limited by aberrations of the eye. Using adaptive optics, a technique borrowed from astronomy, scientists at the University of Rochester were able to neutralize ocular aberrations and photograph individual photoreceptors *in vivo* (Liang, Williams, & Miller, 1997). A better knowledge of the eye's aberrations may also help us understand the etiology of visual anomalies such as myopia or amblyopia (Atchison, Collins, Wildsoet, Christensen, & Waterworth, 1995; Collins, Wildsoet, & Atchison, 1995). New technologies are providing us with the tools to study visual optics in ways that were never before possible. Given the importance of the cornea and the availability of videokeratoscopy, a logical place to begin new research on the eye's optical system is the

cornea.

## 3.2

### CORNEAL SHAPE

#### 3.2.1 Mean shape of the human cornea

Viewed from the front, the cornea is slightly oval, with vertical and horizontal dimensions of approximately 11 and 12 mm, respectively (Last, 1968). Normally, pupil diameter ranges from 3-6 mm, and this limits the optical zone of the cornea to the central 6 mm under most conditions (Holladay & Waring, 1992). In profile, most corneas are nearly circular near the center, with an average apical radius of curvature of about 7.8 mm. The normal range is 7-8.5 mm. The horizontal radius is usually 0.05-0.25 mm flatter than the vertical (with the rule astigmatism) (Gullstrand, 1924). This equates to 0.25-1.25 diopters (D) of corneal astigmatism; average corneal astigmatism is about 0.70 D. In general, the mean apical radius decreases with higher myopia (Carney & Henderson, 1993; Carney, Mainstone, & Henderson, 1997).

#### 3.2.2 Two dimensional models of the general corneal shape

Beyond the paraxial region, the corneal normally flattens, and a useful first order approximation of the typical corneal profile is an ellipse (Mandell & St Helen, 1971; Howland, Buettner, & Applegate, 1994; Mandell, Klein, & Corzine, 1998). Figure 3.1 shows the general features of an ellipse that you might see in a textbook on analytical geometry. The origin is placed at the center of the ellipse, and the major axis lies on the x axis, while the minor axis is on the y axis. An ellipse is defined (Washington, 1986) as “the locus of a point P(x,y), which moves so that the sum of its distances from two fixed points is constant.” These two fixed points, called foci, are located at coordinates (-c,0) and (c,0) in Fig. 3.1. The eccentricity (e) parameter describes the degree of elongation of an ellipse and may be defined by the ratio of the distances, c and a:

$$e = c / a \quad (3-1)$$

The eccentricity of an ellipse has a value,  $0 < e < 1.0$ , where a value of  $e = 0$  represents a sphere, and a value of  $e = 1.0$  is associated with another conic section, the parabola (Benjamin & Rosenblum, 1992).

Baker’s formula (1943), Eq. (3-2), is another general mathematical expression for conic sections, including ellipses, and has been popular among vision scientists for modeling the general corneal profile (Bennett & Rabbetts, 1989a; Burek & Douthwaite, 1993; Lam & Douthwaite, 1994; Salmon & Horner,

1995) in two dimensions (Fig. 3.2). This formula places the origin at the corneal apex and can describe a wide range of normal corneal shapes by varying just two parameters, the apical radius ( $r$ ) and shape factor ( $p$ ). The value of  $p$ , is related to the conic eccentricity ( $e$ ) by Eq. (3-3).

$$y = \sqrt{2rx - px^2} \quad (3-2)$$

$$p = 1 - e^2 \quad (3-3)$$

A shape factor of  $0 < p < 1$  describes a prolate, or flattening ellipse. The portion of an ellipse at either end of the major axis is prolate in shape, since the local curvatures gradually flatten with departure from the vertex. A value of  $p = 1.0$  indicates a sphere, and  $p > 1.0$  indicates an oblate or steepening ellipse. The portion of an ellipse at either end of a minor axis is oblate in shape, since the local curvatures gradually steepen for points departing from the minor vertices.

The mean corneal shape factors ( $p$ ) reported in several corneal topography studies were between 0.74 and 0.89, and the range of reported values was 0.19-1.47 (Eghbali, Yeung, & Maloney, 1995). These are summarized in Table 3.1. Though most normal corneas are similar to prolate ellipsoids, 5-20% may be oblate (Eghbali, *et al.*, 1995; Carney, *et al.*, 1997). Refractive surgery usually produces an oblate surface, which is flat centrally and steep peripherally. Shape factors may vary with meridian, and Eghbali found an average standard deviation of 0.17, though no specific trend was identified (Kiely, Smith, & Carney, 1982).

Referencing work by Bonnet, Lotmar developed a polynomial expression for an aspheric model cornea (Lotmar, 1971):

$$x = \frac{y^2}{2r} \left[ 1 + \frac{5}{28} \left( \frac{y}{r} \right)^2 - \frac{1}{12} \left( \frac{y}{r} \right)^4 \right] \quad (3-4)$$

Variable  $r$  represents the apical radius of curvature,  $y$  is the radial distance from the center, and  $x$  is the surface elevation. An ellipse with a 7.8-mm apical radius ( $r$ ) and shape factor ( $p$ ) of 0.6 matches Lotmar's formula within  $1.0 \mu\text{m}$  across a 6.0 mm diameter zone, so Lotmar's model cornea is close to an ellipse.

A rotationally symmetric ellipsoid provides a realistic model cornea that can predict many of its optical properties. As will be discussed in more detail later (Section 3.5.1), toricity can be added to better simulate a real cornea (Burek & Douthwaite, 1993; Salmon & Horner, 1995). Applegate hypothesized that

the corneal shape tends to become more spherical (p value approaches 1.0) in high myopia (Applegate, *et al.*, 1994), and this relationship was verified in another study of 113 eyes (Carney & Henderson, 1993). Chapter 5 contains more detail on the computation of corneal optics from topography.

**TABLE 3.1** Corneal shape factors (p) reported in various studies (Eghbali, *et al.*, 1995; Carney, *et al.*, 1997).

Study	# eyes	Shape factor (p)	Comment
Townsend (1970)	350	.75	range .19-.84
Mandell (1971)	8	.76	range .27-.96
Bibby (1976)	2,100	.85 ±.18	
Bibby (1976)	32,000	.79 ±.15	horizontal meridian
Kiely (1982)	176	.74 ±.18	range .24-1.47
Kiely (1984)	196	.79 ±.19	range .24-1.47
Guillon (1986)	220	.83 ±.13 / .81 ±.16	flat / steep meridian; range .21-1.20
Sheridan (1989)	56	.88	
Carney (1997)	113	.69 ±.23	range .03-1.29

### 3.3

#### HISTORY OF QUANTITATIVE CORNEAL MEASUREMENT

##### 3.3.1 Keratometry

The most widely used instruments for measuring corneal curvature are the keratometers, sometimes called ophthalmometers. In 1796, Ramsden built an apparatus to measure corneal curvature to determine if the cornea changes during accommodation (Mandell, 1960). His instrument employed a telescope to magnify the image of mires reflected off the corneal surface. As with modern keratometers, a doubling device was used to allow stable measurement in spite of microscopic eye movements. Ramsden's work was largely forgotten, but a generation later other scientists began to build similar devices for measuring the curvature of the central cornea. Kohlrausch, in 1839, built an instrument that included a telescope and size adjustable luminous mires. In 1854, Helmholtz added a doubling device, as Ramsden had done earlier, to

eliminate the problem of an unstable image caused by eye movements; he is usually credited with the invention of the keratometer. The Helmholtz ophthalmometer measured the curvature of the cornea and other optical surfaces of the eye as well. In 1881, Javal and Schiötz improved Helmholtz' laboratory apparatus and built an ophthalmometer designed for clinical use. With only minor changes, the same design is still in use today as the Haag-Streit ophthalmometer.

The Javal-Schiötz instrument and the many that have followed it are designed expressly to determine the curvature, and particularly the astigmatism, of the cornea only. It would thus appear appropriate to call them keratometers (cornea measurers), leaving the terms ophthalmometer and ophthalmometry for the wider field of investigation of the refracting surfaces of the eye generally. (Emsley, 1946).

Bausch & Lomb added several useful features to their keratometer, which was introduced in 1932. It included a Scheiner's disk to improve focusing, circular mires to allow better qualitative assessment of the corneal surface, and the capacity to measure two orthogonal corneal meridians simultaneously. The Bausch & Lomb keratometer, now manufactured by Reichert, has remained essentially unchanged since 1932. Along with copies built by other companies, this is the most popular clinical instrument for measuring corneal curvature.

For nearly a century, clinicians relied almost exclusively on keratometry for quantitative corneal surface data. As an adjunct to refraction and for contact lens fitting, the keratometer was adequate for most normal corneas. Keratometry also proved valuable for other applications, such as the calculation of intraocular lens power, or in the management of surgically induced astigmatism. Modern computerized corneal topographers are closely tied to the keratometer tradition, and they usually provide simulated keratometer data along with their color maps.

### **3.3.2 Keratoscopy**

Using keratoscopy, it is possible to examine a much greater area of the cornea than is possible with keratometry. Clinical keratoscopy has been used since 1870, when Placido studied the corneal surface by observing the shape of concentric rings reflected off the cornea (Fig. 3.3). Most modern videokeratoscopes are based on the same principle, and use a pattern of reflected rings, called a Placido's disk. Depending on the size of the Placido's disk, it is possible to qualitatively evaluate most of the corneal surface. Various keratoscope designs were developed for clinical and surgical use, and until recently, they provided only a gross qualitative assessment of the cornea.

In the 1880's, Javal recognized the importance of recording the keratoscope image photographically (Reynolds, 1992), and in 1896, Gullstrand developed the first photokeratoscope. This opened the way for

detailed mathematical analysis of corneal shape, and Gullstrand developed algorithms to derive quantitative data from careful measurements of the keratograph rings (Gullstrand, 1966). Unfortunately, until recently, the process was too tedious to be clinically useful. In the 1970's, several photokeratoscopes were designed with attached Polaroid cameras. One version, the Corneoscope (Fig. 3.3), and its companion device for image analysis, the Comparator, allowed fast, in-office evaluation of the Polaroid keratograph (Lundergan, 1992). These instruments were used primarily for advanced contact lens fitting and did not become widely accepted among clinicians, who continued to rely on the simpler, more familiar keratometer.

In the 1980's, keratorefractive surgery provided the impetus to develop better corneal topographers, but a major obstacle continued to be the volume of data and tedious data analysis (Klyce & Wilson, 1989). While keratometry evaluates the cornea based on four paracentral points, modern computerized videokeratoscopes evaluate thousands of points covering most of the cornea. Advances in video and personal computer technology made it possible to instantaneously acquire and analyze high quality images. These improvements made quantitative keratometry practical for routine clinical use (Koch & Haft, 1993). Since 1987, color topographic maps have been the standard method for displaying computerized videokeratographic data (Maguire, Singer, & Klyce, 1987). The Corneal Modeling System (CMS) produced by Computed Anatomy (Gormley, Gersten, Koplin, & Lubkin, 1988), became the first widely used computerized videokeratoscope. With instrument improvements, reduced costs and a greater demand for precise corneal information, newer generations of computerized videokeratoscopes came into widespread use in the early 1990's.

### 3.3.3 Other technologies

In an effort to improve accuracy and avoid the assumptions necessary to compute three-dimensional surface estimates from two-dimensional Placido images, one videokeratoscope, the EyeSys System 2000 (EyeSys Vision Group, formerly EyeSys Technologies), shown in Fig. 3.4, added side cameras which view the cornea in profile. Some companies developed non-Placido methods for measuring the corneal surface. The PAR Corneal Topography System (PAR Vision Systems Corporation) uses a rasterstereographic principle (Arffa, Warnicki, & Rehkopf, 1989) to locate a square grid of surface points by stereo-triangulation (Belin, Cambier, Nabors, & Ratliff, 1995). Employing different technology, the ORBSCAN (ORBTEK, Inc.) rapidly scans a sequence of optical slits across the cornea, and analyzes these images to reconstruct the anterior and posterior corneal surfaces. The CLAS 1000 (Eye Technology, Inc.) is based on laser holographic imaging and provides very high resolution corneal surface maps without reliance on projected patterns. The University of Masstricht, in the Netherlands, recently developed a "Fourier Profilometry" method, which is the basis for the Euclid ET-800 Corneal Topography System (Euclid Systems Corporation), the newest entry in the corneal topography market. These alternate

technologies possess theoretical advantages (Applegate & Howland, 1995), but videokeratography is still the most popular method for mapping the corneal surface.

## 3.4

### VIDEOKERATOSCOPE RECONSTRUCTION ALGORITHMS

#### 3.4.1 Limitations based on instrument design

While trying to construct an accurate topographic map of the cornea, all videokeratoscopes face inherent problems that can introduce error, and these must be minimized by the instrument design and data processing (Applegate, 1992). Instrument design considerations include the working distance and size of the illuminated Placido's disk. Interestingly, the two major manufacturers have taken opposite approaches to instrument design with regard to these factors. The Tomey (formerly Computed Anatomy) Topographic Modeling System (TMS-2) uses a small target with a short working distance. This maximizes corneal coverage and allows for a smaller instrument, but the short working distance is very sensitive to focus and alignment errors (Applegate & Howland, 1995). Tomey's main competitor, EyeSys, chose a different approach. The EyeSys 2000 Corneal Analysis System uses a larger target and longer working distance. These reduce the effects of focusing and alignment errors (Mandell & Horner, 1993) but require a larger Placido's disk, which may be partially obscured by the patient's nose or brow. Reconstruction algorithms require that the entire Placido's disk image be in focus at the videokeratoscope working distance, but it is impossible for all the keratoscope rings to be focused in the same plane for all corneas. The shape of the keratoscope face is designed to minimize this source of error. Also, the concentric ring target has inherent limitations. It cannot measure the cornea inside the central ring, and though designed to collect data along radial meridians (Fig. 3.5), these targets provide no information about corneal shape in the circumferential direction (Applegate, 1994; Rand, Howland, & Applegate, 1997). In spite of these limitations, algorithms have been developed which minimize error and allow noninvasive measurement of the cornea, which is sufficiently accurate support a wide range of clinical and research applications.

#### 3.4.2 Overview of corneal reconstruction algorithms

The process of building a topographic map of the cornea from keratoscopic data goes through the following general steps:

- 1) Capture a video image of the keratoscope rings.
- 2) Measure the angular size at discrete points on each ring.
- 3) Mathematically reconstruct the corneal surface point by point.

- 4) Compute an appropriate index to describe each surface point.
- 5) Create a pseudocolor map to show these indices across the cornea.

Clark (1973) published a comprehensive historical review of photokeratoscopy and their mathematical analyses that covered the work of Gullstrand through the developments of the early 1970's. Since then, several important articles describing keratoscope algorithms have appeared (Doss, Hutson, Rowsey, & Brown, 1981; Klyce, 1984; Wang, Rice, & Klyce, 1989; van Saarloos & Constable, 1991; Klein, 1992; Halstead, Barsky, Klein, & Mandell, 1995; Klein, 1997b). The actual algorithms used by the commercial instruments are closely guarded secrets, and they may not be the same as those that appear in the open literature. Nevertheless, it is beneficial to study published algorithms, since they clarify the basic methods used to reconstruct the corneal surface from videokeratographic data.

Corneal reconstruction begins with analysis of the rings contained in the videokeratograph. A polar coordinate system is imposed on the image, and each point on a ring is specified by its meridian and distance from the center (Fig. 3.6). The objective of the algorithm is to estimate the location, in three-dimensional space, of the corneal surface points that gave rise to the image. By analyzing the cornea meridian by meridian, these instruments simplify analysis by treating the surface as a set of many two-dimensional radial profiles. It is important to note that this approach treats each meridian as one slice out of a rotational symmetric surface. In this geometry, the incident and reflected rays remain in the same plane. Most corneas, however, are not rotationally symmetric, so this simplifying approximation of corneal shape can introduce errors, depending on the actual shape of the cornea. For example, in a toric cornea, the incident and reflected rays are coplanar for the principal meridians only, but in oblique meridians the reflected rays are always skewed out of the incident plane. For the range of toricities seen in normal corneas, however, the skew ray error is negligible (Hilmantel, Blunt, Applegate, & Howland, 1997; Klein, 1997a). Therefore, except for severely distorted corneas, two-dimensional reconstruction algorithms are accurate enough for most clinical applications.

### 3.4.3 The van Saarloos algorithm

Newer videokeratoscopes have turned to “arc-step” reconstruction methods, and van Saarloos wrote a summary of one such algorithm (van Saarloos & Constable, 1991). Considered in two-dimensions, the keratoscope rings represent object points located at different distances from the optic axis, and after reflection off the corneal surface, chief rays can be traced through the camera nodal point to its corresponding image point in the camera image plane (Fig. 3.7). The known position of each object point, the camera working distance (wd) and angular size of each image point ( $\alpha$ ) are required to compute the corneal reflection points. Unfortunately, as shown in Fig. 3.7, without additional assumptions, this does

not lead to a unique solution (Wang, *et al.*, 1989). This algorithm requires the following constraints to determine a unique location for each reflection point.

- Successive corneal points are joined by small circular arcs.
- Adjoining arcs have a single slope value at their junctions.

The van Saarloos algorithm uses several iterative calculations to refine the estimate of each reflection point. Figure 3.8 shows the geometry, and the algorithm is summarized by the following steps, each of which includes numerous iterations.

- 1) Estimate the corneal apical radius ( $r$ ).
- 2) Calculate coordinates for the first corneal reflection point and its slope.
- 3) Using data for the previous point, calculate the coordinates and slopes for subsequent reflection points.
- 4) Repeat the process for the next meridian.

Readers may refer to the article (van Saarloos & Constable, 1991) for the details of this algorithm. Two misprinted equations in that article have been corrected in the footnote below<sup>a</sup>.

#### 3.4.4 The Klein algorithm

A shortcoming of arc-step algorithms is that corneal points are connected with circular arcs that have abrupt changes in curvature at each point. Klein designed an algorithm which connects the corneal reflection points with a smooth continuous curve that better models the corneal surface (Klein, 1992). As with the previously described algorithm, calculations are based on the angular height of each reflection point, and two constraints, listed below, are necessary to limit the answer to a unique point.

- The surface is modeled by a cubic polynomial curve.
- The sampled surface point is located at the intersection of the reflected ray and the calculated polynomial curve.

This efficient iterative algorithm can be implemented with a few lines of computer code, and a BASIC program is included in Klein's paper. Referring to the geometry of Fig. 3.9, this algorithm is summarized as follows:

- 1) Estimate the first reflection point position ( $a$ ) on the reflected ray, directly above the

---

<sup>a</sup> In the left column of page 961, the bottom equation should read,  $\theta = 1/2[(2\phi - \alpha) - \alpha]$ . On page 962, the equation on the last paragraph, first line should read,  $1/2(wd + d_0 - y_{i-1})$ .

corneal apex.

- 2) Compare the incident ray-normal angle with the reflected ray-normal angle at this point. If the first angle is larger than the second, increment along the reflected ray for a better estimate of the reflection point (b).
- 3) Calculate the polynomial curve joining the apex and point (b).
- 4) Repeat steps 2) and 3) until the incident and reflected angles become equal within a predetermined tolerance.
- 5) Using data for this reflection point, calculate subsequent points similarly.
- 6) Repeat for the other meridians.

These algorithms illustrate the process by which three-dimensional coordinates for corneal surface points are computed using two-dimensional algorithms. This is repeated for all semi-meridians in small radial increments. Depending on the videokeratoscope, 5,000-10,000 points may be computed to reconstruct the corneal surface. More recently, Halstead published a unique three-dimensional algorithm (Halstead, *et al.*, 1995), which reconstructs the cornea by analyzing data for the entire surface without geometric constraints. A rough computer simulation of the cornea surface is constructed, and successive iterations improve the correspondence between the real and simulated cornea by analyzing a theoretical keratograph for the simulated surface. Even in 1999, the major videokeratoscopes still use two-dimensional reconstruction algorithms, but future instruments may turn to three-dimensional routines, such as Halstead's, to more accurately compute cornea surface shape.

## 3.5

### CORNEAL TOPOGRAPHIC MAPS

Computerized videokeratoscopy provides a tremendous volume of information about the corneal surface. By representing the data in the form of a color map, the experienced clinician can quickly evaluate corneal shape or other features closely associated with shape. A variety of corneal surface descriptors may be used, so different kinds of color maps can be created for any cornea. The type of map that is used in most clinical situations is the axial curvature map. Sometimes it is better to show the instantaneous curvature, surface elevation or refractive power distribution across the cornea. The following sections explain the principles of each of these kinds of maps.

#### 3.5.1 The ellipsotric model cornea

A reasonable, relatively simple mathematical model of a general cornea is an ellipsotric surface

(Burek & Douthwaite, 1993). The corneal profile in each meridian is an ellipse described by Baker's formula Eq. (3-2). Equation (3-5) is equivalent except that variable  $y$  has been replaced with the Greek letter  $\rho$  (rho), and the former variable,  $x$ , has been replaced by  $z$ . The ellipsoidal profile (Eq. 3-5) may be then applied to any radial meridian, in a cylindrical coordinate system, such that variable  $\rho$  represents radial

$$\rho = \sqrt{2r_{\theta}z - pz^2} \quad (3-5)$$

distance from the optic axis,  $z$  specifies distances in the direction of the optic axis, and  $r_{\theta}$  is the apical radius of curvature in the meridian of interest. It is possible to specify a different shape factor,  $p$ , for each meridian, but for simplicity I kept the  $p$  value constant for all meridians. The variables are illustrated in Fig. 3-10. In creating a mathematical model of the cornea, all variables except  $z$  are usually defined ahead of time, and it is necessary to solve for  $z$ . Equation (3-6) solves for  $z$  in terms of the other variables.

$$z = \frac{r_{\theta} - \sqrt{r_{\theta}^2 - p\rho^2}}{p} \quad (3-6)$$

All that remains to define a model cornea in three-dimensions is a describing function for variable  $r_{\theta}$ . This is shown by Eq. (3-7), which interpolates meridional curvature ( $1/r_{\theta}$ ) based on user defined values for the maximum ( $r_h$ ) and minimum ( $r_v$ ) radii. When modeling a with the rule cornea,  $r_h$  is the radius of curvature in the horizontal (180 degree) meridian, and  $r_v$  is the radius of curvature in the vertical (90 degree) meridian. Equation (3-7) is based on the familiar optometric principle that the apical curvature in an oblique meridian of a toric surface varies as a sine squared function of the oblique angle (Churms, 1981).

$$\frac{1}{r_{\theta}} = \left[ \frac{1}{r_h} \cos^2 \theta + \frac{1}{r_v} \sin^2 \theta \right] \quad (3-7)$$

Based on Eqs. (3-6) and (3-7), a simple computer program may be written to generate cylindrical coordinates ( $\rho$ ,  $\theta$ ,  $z$ ), for a surface that includes two important features of a generalized cornea—an ellipsoidal flattening profile, and corneal toricity, as defined by input variables,  $r_h$  and  $r_v$ . This model

(Salmon & Horner, 1995) is appealing from an optometric point of view since the two variables,  $r_h$  and  $r_v$ , are the same parameters that are routinely recorded in clinical keratometry. The example corneal maps in Figs. 3.11, 3.12 and 3.13 are based on this ellipsotric model, with  $r_h = 8.00$  mm,  $r_v = 7.50$  mm and a constant shape factor ( $p$ ) of 0.85. This represents a cornea with 2.81 D of astigmatism. The relatively large astigmatism was selected to better illustrate the difference between the various kinds of corneal maps used on today's videokeratoscopes.

### 3.5.2 Surface elevation maps

Since surface shape is the primary determinant of corneal optics (Applegate, 1994; Applegate & Howland, 1995), a logical way to map the cornea is to show the surface elevation of each point, relative to a reference surface. With topographic land maps, elevations are measured from a reference "plane" at sea level. However, for the cornea, elevations measured from a plane are nearly useless, because even minute changes in elevation (on the order of micrometers) can be optically significant, but these are lost in the larger total height of the cornea (Klyce & Wilson, 1989; van Saarloos & Constable, 1991; Holladay & Waring, 1992). A better method for presenting the true topography (surface elevation) is to measure from a reference sphere, ellipsoid or other surface that approximates the general corneal shape (Salmon & Horner, 1995). Figure 3.11 shows four surface elevation maps for the 2.81 D with the rule astigmatic model cornea, mentioned above. Elevations were measured relative to a plane as well as to a flat, median and steep reference spheres. Note that surface toricity is readily apparent when reference spheres are used but it cannot be distinguished when elevation is measured relative to a plane.

### 3.5.3 Dioptric curvature maps

Most corneal topography systems do not plot surface elevations, but describe the surface in terms of dioptric values. These dioptric maps are popular because they use the terminology of keratometry, with which clinician are familiar (Roberts, 1994a). Just as different elevation maps of the same cornea can be drawn, dioptric data for the same surface can also be expressed in different ways (Klein, 1992; Mandell, 1992). In optometry, diopters are sometimes used to quantify surface curvature; in other cases diopters express surface refractive power. Near the corneal apex, surface curvature and power are so closely related that they are sometimes treated synonymously. When the data are appropriately scaled, this works for keratometry, since measurement are limited to the paraxial region. However, outside the paraxial zone, it is important to make a distinction between dioptric curvature and dioptric power. Three kinds of dioptric curvature maps will be described in the following paragraphs. These include the axial and instantaneous maps, which are available on most commercial instruments used today and a new type of map called the

Gaussian curvature map.

As was mentioned in Section 3.4.1, all current videokeratoscopes map the three-dimensional corneal surface by applying the two-dimensional geometry of Fig. 3.10 to each corneal meridian. In effect, this assumes that the surface normal for each surface point intersects the videokeratoscope axis. This is not strictly true for most meridians of a non-rotationally symmetric surface, such as a toric cornea or one with keratoconus. The error in axial curvature caused by this simplifying assumption is clinically negligible for normal corneas with regular astigmatism, but for abnormally shaped corneas, as seen in keratoconus or following refractive surgery, the error can be large (Klein, 1997c). Since the purpose of this chapter was to explain and compare the basic types of corneal maps produced by current machines, I resort to the same two-dimensional geometry assumed by all modern videokeratoscopes. This simplifying assumption is also used with the refractive power maps described in Section 3.5.4.

#### a. Axial curvature maps

As illustrated in Fig. 3.10, it is possible to define a local radius of curvature for a corneal surface point (B) as the distance from that point to the optic axis along the normal ( $BC_a$ ). This is the same radius that is measured in keratometry (Bennett & Rabbetts, 1989c; Mandell, 1994), and this definition assumes that the center of curvature ( $C_a$ ) is located on the optic axis. The radius ( $BC_a$ ) thus derived is called the *axial* radius of curvature ( $r_a$ ). It is sometimes also called the sagittal radius, though this is technically correct only for a rotationally symmetric surface (Applegate, 1994). The center of curvature for all surface points lies on the optic axis for spherical surfaces only, and since most corneas are nearly spherical near the apex, this assumption is acceptable for keratometry. However, this assumption introduces major errors in the periphery of an asphere. In the example of an ellipse, the center of curvature for more peripheral points gradually departs from the optic axis (Roberts, 1994b). In the ellipsotopic model, we can compute the axial radius ( $r_a$ ) of curvature from Eq. (3-8) (Bennett, 1988; Douthwaite, 1995; Salmon & Horner, 1995). Equation (3-8) is based on Baker's equation (Eq. 3-2 and 3-5), and the derivation is presented in Appendix B.

$$r_a = \sqrt{r_\theta^2 + (1 - p) \rho^2} \quad (3-8)$$

The radius ( $r_a$ ) in meters is usually converted to dioptric curvature ( $K_a$ ) using the keratometer formula (Eq. 3-9). In this way, curvature values across the cornea are computed, and these may be presented in an axial curvature map such as that shown in Fig. 3.12a. Axial curvature maps are the default map used in most

clinical instruments.

$$K = \frac{(1.3375 - 1.0)}{r} \quad (3-9)$$

### b. Instantaneous curvature maps

If the goal is to describe the local curvature within the meridional plane (plane of the page in Fig. 3.10), the axial, or keratometer based radius will be correct for a sphere but incorrect for an asphere such as an ellipse. For this reason, many computerized videokeratoscopes provide another estimate of local curvature that is based on the standard definition for curvature from plane geometry. In the jargon of modern videokeratoscopy, this is called the *instantaneous, tangential*, or sometimes *meridional* radius of curvature, and is represented by segment  $BC_i$ . The formula to compute the instantaneous radius for a two-dimensional function is shown in Eq. (3-10). It uses the first ( $dp/dz$ ) and second ( $d^2p/dz^2$ ) derivatives of the equation for the curve (Eq. 3-6) to calculate this local radius ( $r_i$ ):

$$r_i = \frac{\left[1 + \left(\frac{dp}{dz}\right)^2\right]^{\frac{3}{2}}}{\pm \left(\frac{d^2p}{dz^2}\right)} \quad (3-10)$$

In the case of an ellipsoid, if the apical radius ( $r_\theta$ , or  $AC_0$ ) and axial radius ( $r_a$ ) are known, the instantaneous radius ( $r_i$ ) is easily calculated from the following relationship (Bennett & Rabbetts, 1989b):

$$r_i = \frac{r_a^3}{r_\theta^2} \quad (3-11)$$

For a prolate ellipse, which is similar to most corneas, the instantaneous radius is increasingly longer than the axial radius for more peripheral points. As with the axial radius, the instantaneous radius is usually converted to dioptric curvature using the keratometer formula (Eq. 3-9). Figure 3.12 compares an instantaneous curvature map (Fig. 3.12b) with an axial curvature map (Fig. 3.12a) for same model cornea.

The axial and instantaneous curvature maps describe features of the cornea that are familiar to most clinicians. The apical values are the same on both maps, and these represent either dioptric curvature or power. They both show a decrease in diopters from center to periphery, indicating a flattening contour. In the ellipsoidal example of a with the rule cornea (horizontal principal meridian is flatter), a vertically oriented dumbbell pattern is seen. A major difference between the axial and instantaneous maps of the same cornea is that instantaneous maps show a greater decrease in dioptric values from center to periphery. Computerized videokeratoscopes originally calculated only axial curvature maps, but now most instruments also offer instantaneous (tangential or meridional) curvature maps as well.

### c. Gaussian curvature maps

For a rotationally symmetric cornea, the instantaneous and axial maps represent the minimum and maximum curvatures, respectively, at each point across the cornea. An asymmetric surface will also have maximum and minimum curvatures for any point, and these will always be orthogonal to each other. A group working at the University of California at Berkeley suggested another type of dioptric curvature map, the Gaussian power map (Barsky, Klein, & Garcia, 1997), which displays the geometric mean of these two curvatures across the cornea. This map also includes a vector overlay which shows the orientation of the minimum curvature and the difference between the maximum and minimum curvatures. The Gaussian display offers advantages over the more traditional axial curvature maps; the pattern is shape-invariant, irrespective of the instrument optic axis location, and it better reveals the cone shape in decentered keratoconus.

### 3.5.4 Refractive power maps

Axial and instantaneous maps are based on a local radius of curvature for each corneal point. In paraxial optics, incident light rays are nearly normal to the corneal surface, and in that case, the approximate refractive power of the cornea is inversely proportional to the local radius. The keratometer formula, which converts both axial and instantaneous radii to diopters (Eq. 3-9), uses this assumption to estimate corneal surface “power”. It is incorrect, however, to assume that either axial or instantaneous dioptric maps describe refractive properties of the cornea outside the paraxial region. In that case, it is better to use ray tracing based on Snell’s law to compute the refractive power of the cornea (Camp, *et al.*, 1990; Maguire, *et al.*, 1991).

Roberts summarized the reason why the paraxial formula closely approximates refractive power near the apex only, but not in the periphery (Roberts, 1994a). Assuming the meridional geometry of Fig. 3.10, the refractive power (K) at any point on the corneal surface, through which a ray is traced, is (Klein, 1992):

$$K = n'/(z+f), \quad (3-12)$$

In Eq. (3-12),  $n'$  is the refractive index of the cornea (often taken to be 1.3375), and  $f$  is the axial distance from the point of incidence (P) to the focal point (F') for an off-axis parallel ray. For collimated incident rays, the angle of incidence ( $\theta_i$ ) is defined by Eq. (3-13),

$$\theta_i = \sin^{-1} \left( \frac{\rho}{r_a} \right) \quad (3-13)$$

where  $r_a$  is the axial radius of curvature (Salmon & Horner, 1995). Using Eq. (3-13) and Snell's law (Eq. 3-14), we can solve for the angle of refraction  $\theta_r$  using Eq. (3-15).

$$n(\sin\theta_i) = n'(\sin\theta_r) \quad (3-14)$$

$$\theta_r = \sin^{-1} \left( \frac{\rho}{n'r_a} \right) \quad (3-15)$$

In this case, the index of refraction for the medium of the incident ray ( $n$ ) is equal to 1.0 and  $n'$  is 1.3375. Klein has shown (Klein, 1992) that, for meridional ray tracing, the refractive power of a corneal point can also be defined as:

$$K = \frac{n'}{z+f} = \frac{n'}{z + \frac{\rho}{\tan(\theta_i - \theta_r)}} \quad (3-16)$$

For very small angles, both the sine and tangent of an angle may be approximated by the angle itself (Smith, 1990), and in that case,  $z$  is approximately equal to zero, and Eq. (3-16) reduces to the paraxial equation for surface power (Eq. 3-17 and Eq. 3-9).

$$K = \frac{(1.3375 - 1.0)}{r_a} \quad (3-17)$$

From this, it is clear that the paraxial formula for refractive power (Eq. 3-17) is an approximation of Eq. (3-16), which applies only near the corneal apex, where both the incident angle and sag ( $z$ ) are close to zero. Further from the apex, however, the angle of incidence is too great to be approximated by the angle itself; sag increases and Eq. (3-16) must be used instead of the approximation in Eq. (3-17).

A corneal surface refractive power map based on meridional ray tracing is shown in Fig. 3.13a. Compared to the dioptric curvature maps of the same cornea in Fig. 3.12, the dioptric power map is very different. The dumbbell pattern is now oriented horizontally and, though the apical values are the same, the ray tracing maps shows a large *increase* in dioptric values from center to periphery.

The large increase in power peripherally may be counterintuitive to clinicians who are accustomed to seeing a decrease, but recalling Snell's law and noting that peripheral rays strike the cornea at increasing angles of incidence, it should be no surprise that power increases peripherally. This represents the spherical aberration of the cornea, a peripheral phenomena which will not appear if paraxial equations are used (Salmon & Horner, 1995).

In the mid 1990's some instruments began to incorporate refractive power maps as a display option. An example is the Holladay Diagnostic Summary, provided by the EyeSys 2000 Corneal Analysis System (Holladay, 1995).

Although this is an improvement over the keratometer formula for calculating surface refractive power, meridional ray tracing (Fig. 3.13a) still oversimplifies corneal optics. Small pencils of light refracted through the peripheral cornea do not actually form a single focal point, but an astigmatic interval. This oblique astigmatism is compounded by the toricity and asphericity of the surface. Theoretically, it would be better to represent the power of this cornea with a pair of maps that show the astigmatic sagittal and tangential powers associated with each point (Fig. 3.13). Sagittal and tangential powers were computed by skew ray tracing and the Coddington equations and example maps showing the respective powers are shown in Figs 3.13b and 3.13c (Salmon & Horner, 1995).

### 3.5.5 Comparison of corneal surface descriptors

First generation corneal topography systems offered only axial curvature maps, but newer instruments have added instantaneous (tangential or meridional) curvature maps. Some current instruments also provide surface elevation and ray tracing refractive power displays. These basic descriptors of the

cornea can also be presented in a variety of display formats. Each descriptor shows a different picture of the same cornea, and depending on the specific application, one descriptor may be more useful than another. When an appropriate reference surface is chosen, surface elevation maps reveal details of the corneal surface that may be particularly useful in the pre and post operative management of refractive surgery patients. Surface elevation data was particularly important in this dissertation because it is the information that was used to compute the corneal wavefront aberration. Some instruments that do not display surface elevation maps per se but convey the same information in the form of simulated fluorescein patterns.

Dioptric curvature maps are the most familiar, and they effectively present changes in local contour. They are therefore useful in monitoring surface shape changes, such as those seen in keratoconus or in contact lens induced distortion. The instantaneous curvature map is more sensitive to subtle changes than the axial curvature map, but is also more subject to data noise (Mandell & Horner, 1993; Mandell, Barsky, & Klein, 1994). The axial curvature map may be particularly useful in measuring axially centered surfaces. For example, lathe-cut aspheric contact lenses can be verified using videokeratoscopy (Pole & Sather, 1995). As mentioned above, dioptric curvature maps are sometimes erroneously thought of as refractive power maps. It is important to remind users that, though labeled in diopters, neither axial nor instantaneous maps show local refractive power. Instead, they show a variant of local curvature.

Ray tracing refractive power maps show certain optical effects that are not apparent from any of the other maps, and may therefore be better for visualizing certain optical properties of the surface.

### 3.6

#### **BEYOND TOPOGRAPHY—CORNEAL OPTICS**

When studying corneal optics, it is important to remember that each point in an image is formed by all the light passing through the pupil. Descriptors of corneal optical performance should therefore consider the corneal optical zone as a whole. If the goal is to depict optical performance, other descriptors such as the point spread, optical transfer and wavefront aberration functions may be more appropriate than any of the topographic maps described above. Each of these can be computed from the topography (Hemenger, *et al.*, 1994; Hemenger, Garner, & Ooi, 1995; Oliver, *et al.*, 1997; Oshika, *et al.*, 1999), but these functions are generally not available on current clinical instruments. In Chapter 5, I will use the wavefront aberration function to describe corneal optics. In Chapter 7, I will compare this to the wavefront aberration function for the entire eye and analyze the corneal contribution to the aberrations of the eye.

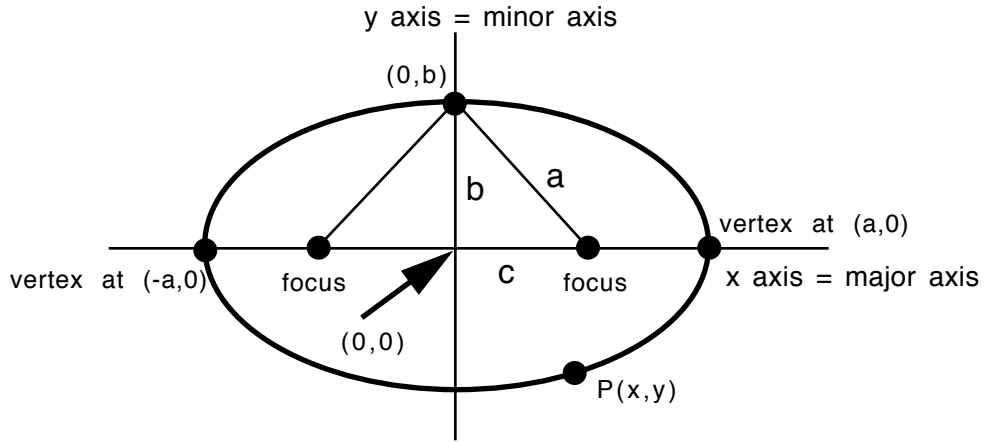


**Figure 3.1**

Basic geometry of an ellipse. The sum of the distance from each focus to any point on the ellipse is a constant value equal to  $2a$ . The parameter describing elongation, eccentricity ( $e$ ), is defined as:  $e = c/a$ ;  $e = 0$  for a circle;  $e = 1$  for a parabola.

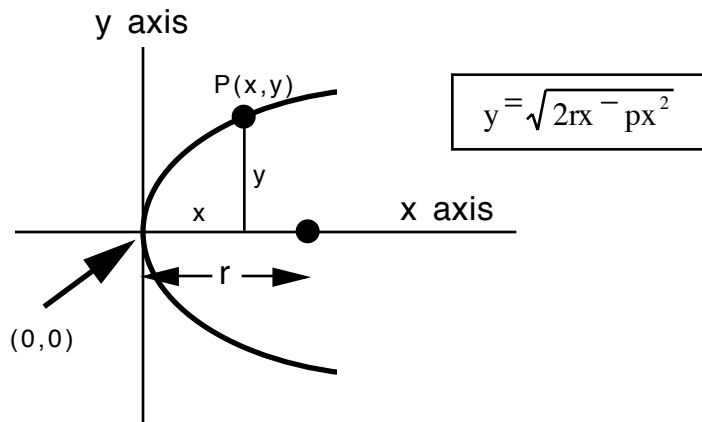


**Figure 3.2**

Coordinate system and variables used by Baker's formula (inset) to trace an ellipse. Variable  $r$  represents the apical radius of curvature.

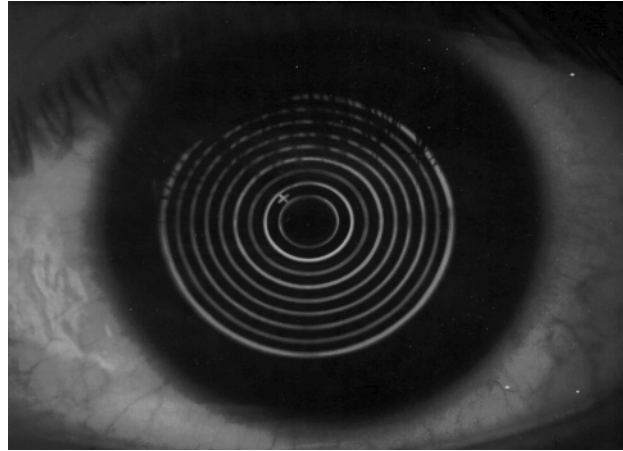


**Figure 3.3**

A Placido's disk or keratoscope consists of a series of concentric illuminated rings that are reflected off the cornea to evaluate its surface shape. The oval shape of the reflected rings is caused by nearly 6 diopters of corneal astigmatism. This image was taken from a Corneoscope polaroid photograph.



**Figure 3.4**

The EyeSys 2000 Corneal Analysis System, one of the most popular computerized videokeratoscopes. (Photograph courtesy of EyeSys Vision Group.)

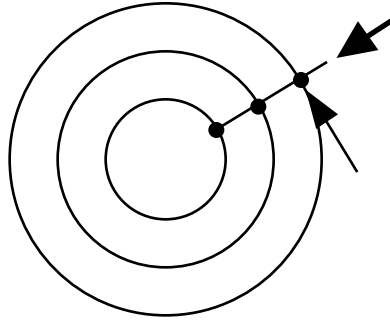


**Figure 3.5**  
Videokeratoscopes measure the cornea at discrete points within multiple radial planes (short arrow) only, but ideally they should also measure in the orthogonal sagittal plane (long arrow) as well.

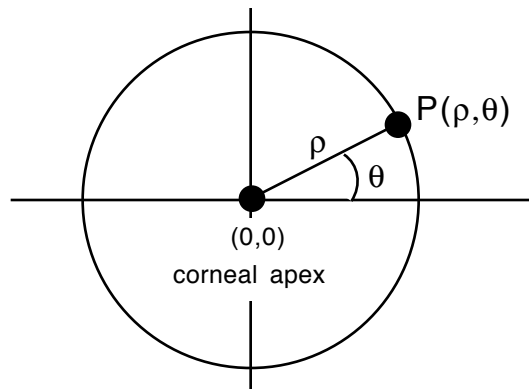


**Figure 3.6**  
A polar coordinate system used with most videokeratoscopes.

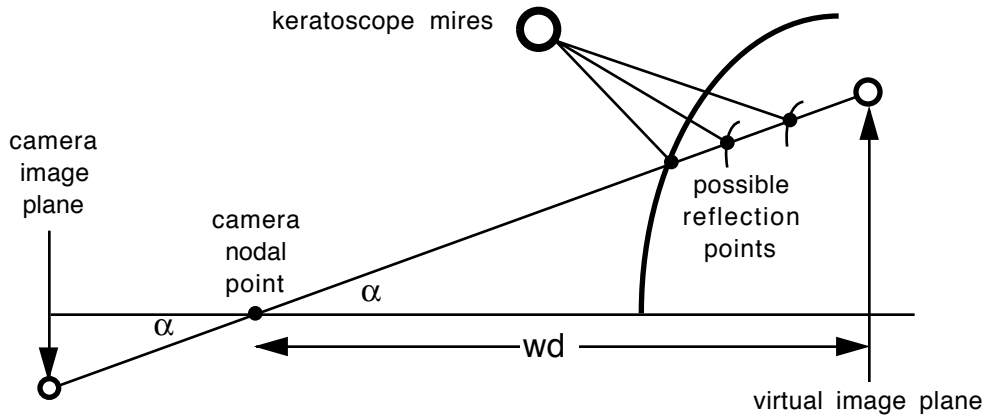


**Figure 3.7**  
 General geometry of videokeratoscopy. The algorithm computes a surface point which may give rise to the reflected image, but without certain assumptions about the surface shape, there is insufficient information to calculate a unique corneal reflection point.

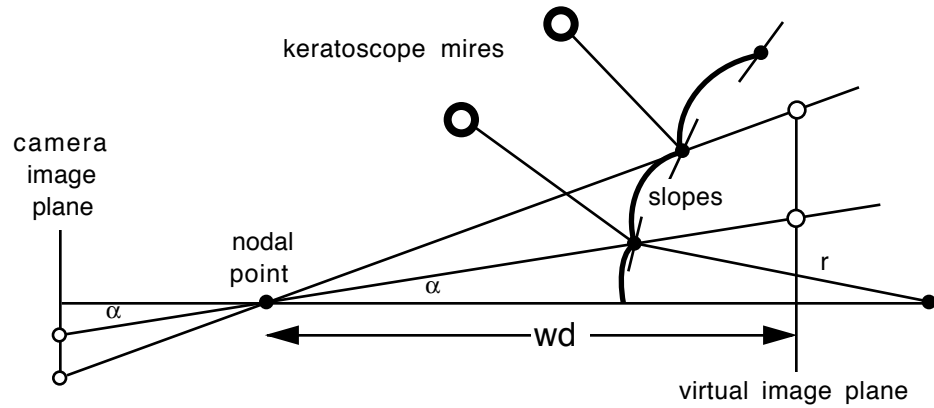


**Figure 3.8**  
 Geometry of the van Saarloos algorithm. Iterative processes estimate corneal reflection points that are joined by circular arcs, which have common slopes at their junctions.

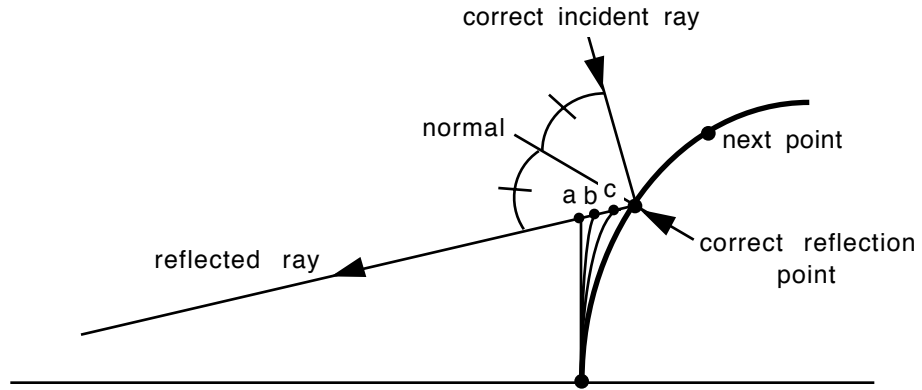


**Figure 3.9**

The Klein algorithm. Successive estimates (a,b,c, ...) of the corneal reflection point are made until the incident and reflected angles become equal. Points are then joined with a smooth cubic spline curve.

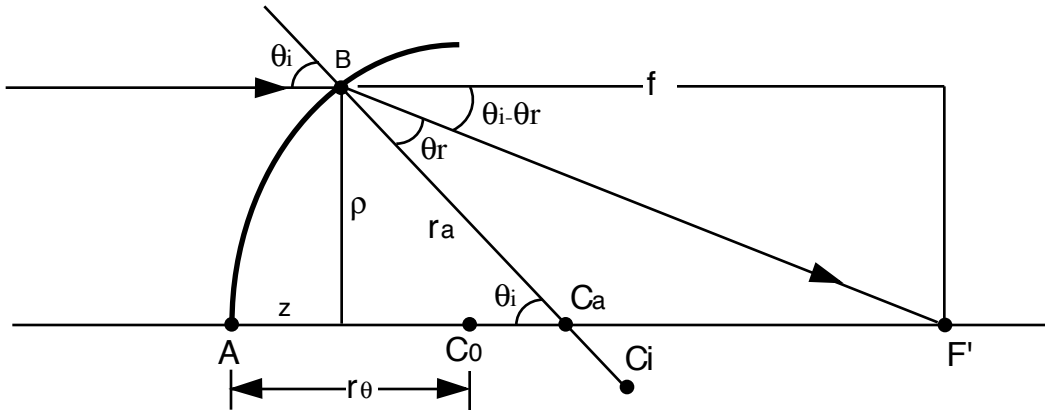


**Figure 3.10**

Two dimensional corneal curve described by Eqs. (3-5) and (3-6). The apical radius of curvature ( $r_\theta$ ) is segment  $AC_0$ ; axial radius ( $r_a$ ) is segment  $BC_a$ ; instantaneous radius ( $r_i$ ) is segment  $BC_i$ . Arrows show the path of rays traced through point B.

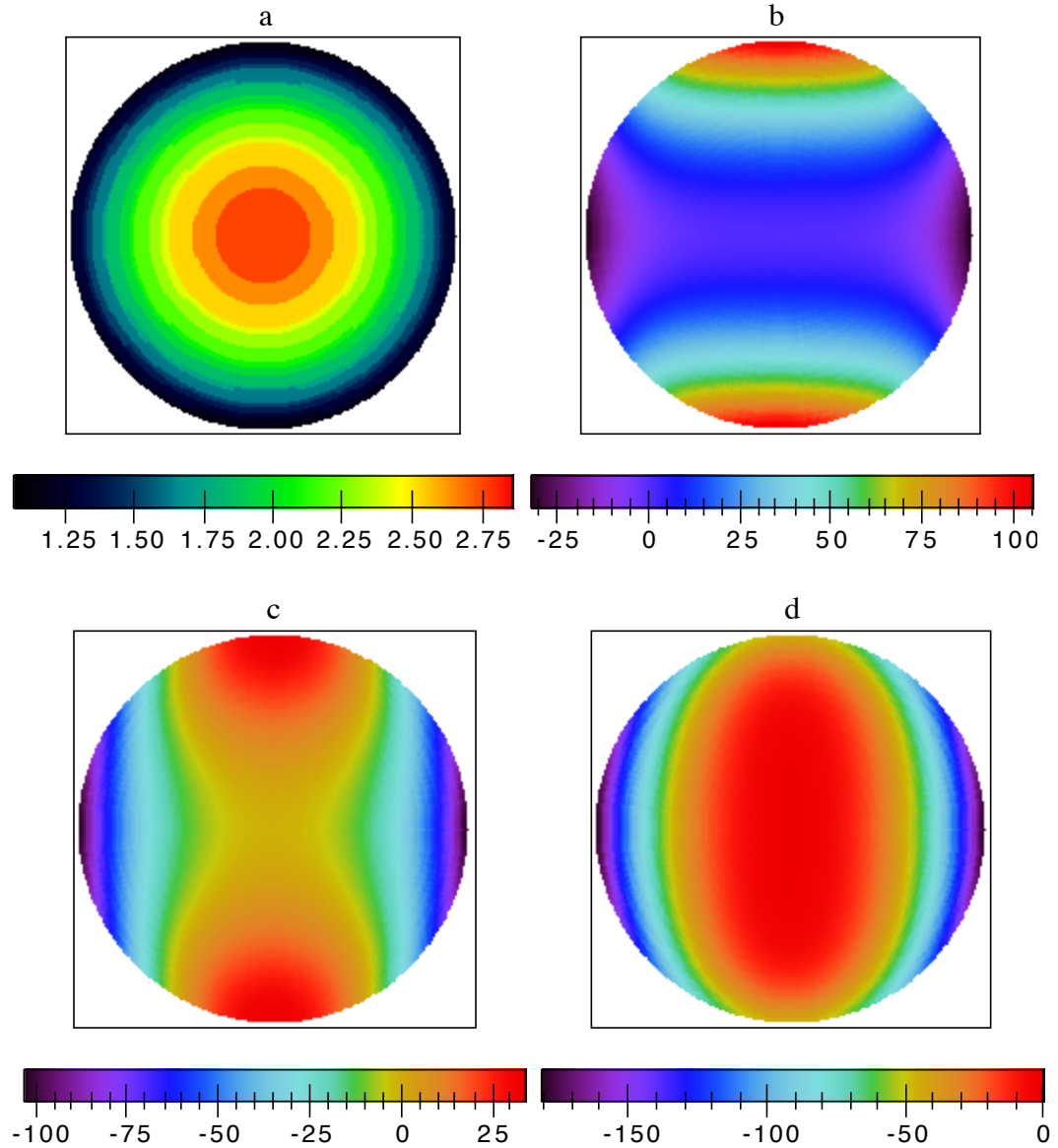


**Figure 3.11**

Four surface elevation maps of a ellipsoidal model cornea, with a horizontal apical radius of 8.00 mm, vertical apical radius of 7.50 mm, and shape factor of  $p = 0.85$ . In (a) elevations are measured from a reference *plane* and the 2.81 D of surface toricity cannot be visualized. The toricity is readily apparent when elevations are measured relative to spherical surfaces, as in (b,c,d). The reference surface in (b) has curvature equal to the flatter, horizontal corneal meridian; the reference surface in (c) has curvature midway between the steep and flat meridians; the reference surface in (d) parallels the steeper, vertical meridian. (Copied with permission: TO Salmon, DG Horner. Comparison of Elevation, Curvature and Power Descriptors for Corneal Topographic Mapping. **Optometry and Vision Science**, 72 (11) 800-808. © American Academy of Optometry 1995)

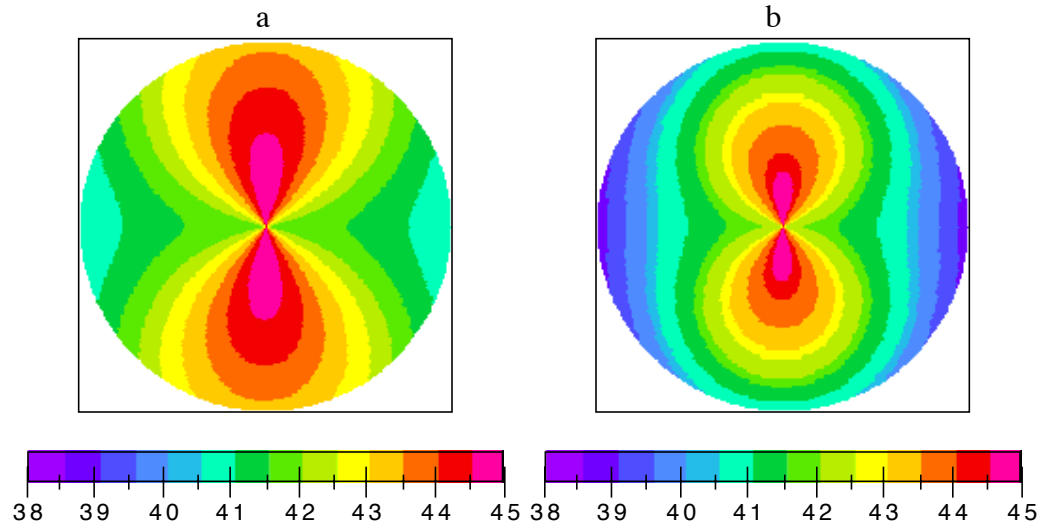


**Figure 3.12**

Axial (a) and instantaneous (b) curvature maps of the same model cornea shown in Fig. 3.10. (Copied with permission: TO Salmon, DG Horner. Comparison of Elevation, Curvature and Power Descriptors for Corneal Topographic Mapping. **Optometry and Vision Science**, 72 (11) 800-808. © American Academy of Optometry 1995)

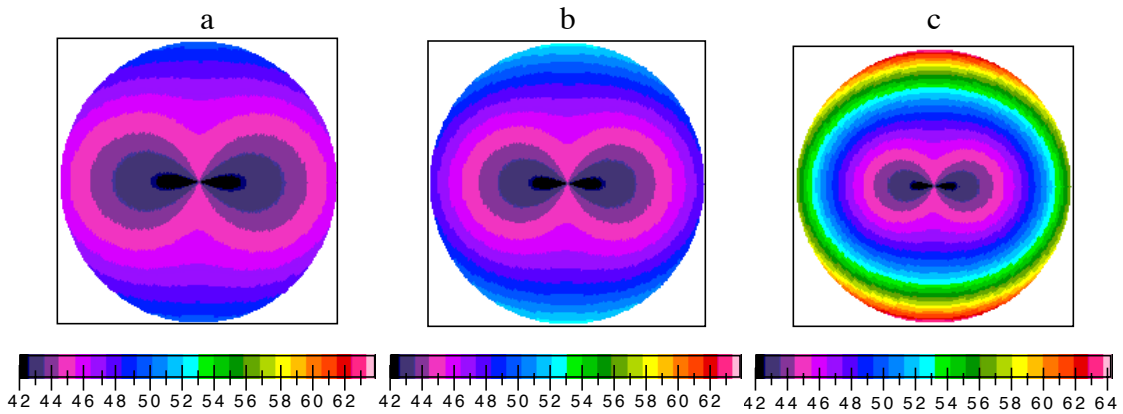


**Figure 3.13**

Refractive power maps based on ray tracing. Map a, above, is based on simple meridional ray tracing; maps b and c are based on skew ray tracing and the Coddington equations. They show the sagittal (b) and tangential (c) powers associated with each corneal point. In contrast to the maps in Fig. 3.12, dioptric power increases from center to periphery. (Copied with permission: TO Salmon, DG Horner. Comparison of Elevation, Curvature and Power Descriptors for Corneal Topographic Mapping. **Optometry and Vision Science**, 72 (11) 800-808. © American Academy of Optometry 1995)